Proceedings of the 8th International Conference on Structural Dynamics, EURODYN 2011
Leuven, Belgium, 4-6 July 2011
G. De Roeck, G. Degrande, G. Lombaert, G. Müller (eds.)
ISBN 978-90-760-1931-4

Design of a low vibration foundation for the nanotechnology hotel Corelab 1B

S. François[1], M. Schevenels[1], G. Lombaert[1], L. Schillemans[2], and G. Degrande[1]
[1]Department of Civil Engineering, K.U.Leuven, Kasteelpark Arenberg 40, B-3001 Leuven, Belgium
[2]Technum-Tractebel Engineering, Van Benedenlaan 73, B-2800 Mechelen, Belgium
email: stijn.francois@bwk.kuleuven.be

ABSTRACT: A nanotechnology facility Corelab 1B is planned on the Arenberg III campus of K.U.Leuven. The Corelab 1B will consist of low vibration floors, cleanrooms and a number of offices. Vibration control in the design stage is of prime concern, since it may cause malfunctioning of sensitive laboratory equipment. The objective of the present paper is the assessment of alternative foundation designs by means of advanced numerical techniques, fully accounting for dynamic soil-structure interaction. A geotechnical characterization of the construction site, including a seismic cone penetration test and an active and passive Seismic Analysis of Surface Waves test, reveals very soft soil layers up to a depth of 8 m. The soil conditions at this site are therefore not ideal for the construction of a nanotechnology facility. Furhermore, the monitoring of the vibration levels at the site show the largest vibration levels arise due to road traffic during rush hours. A three-dimensional coupled finite element boundary element model of the piled foundation of a single floor is constructed, allowing for the assessment of the vibration levels due to traffic on a nearby road. Different foundation designs are analysed. The results are compared to generic vibration criteria and interpreted statistically, taking into account the expected amount of traffic on the nearby road. It is demonstrated that sufficiently stiff piles are required to prevent the large vibration levels in the soft top soil layers to be transmitted to the structure.

KEY WORDS: Dynamics soil-structure interaction; Vibration Criteria; Sensitive equipment

1 INTRODUCTION

A nanotechnology facility Corelab 1B is planned on the Arenberg III campus of K.U.Leuven. The Corelab 1B nanotechnology facility will consist of low vibration floors, cleanrooms and a number of offices. Vibration control in the design stage is of prime concern, since it may cause malfunctioning of sensitive laboratory equipment.

In this paper, the foundation is assessed by means of advanced numerical techniques, fully accounting for dynamic soil- structure interaction.

The paper is structured as follows. In section 2, vibration criteria for sensitive equipment are briefly outlined. The dynamic soil properties and ambient vibration levels at the construction site are discussed in section 3. In section 4, the incident wave field due to the passage of a truck on a nearby road is computed and vibration levels are assessed. The incident wave field is used as an input for coupled finite element (FE) - boundary element (BE) calculations for the dynamic response of the foundation in section 5. In section 6, two alternative foundation designs are studied and the vibration levels during the passage of a truck on the nearby road for the alternative foundation designs are compared to the vibration levels in the original design.

2 GENERIC VIBRATION CRITERIA

Vibration criteria for sensitive equipment can broadly be classified as tool specific and generic criteria. If a specific area is evaluated for particular sensitive equipment, vibration criteria provided by the manufacturer should be considered. In the early stages of design, when the equipment is not yet selected, generic vibration criteria are used instead [1].

Generic vibration criteria are generally formulated in terms of narrow band or one-third octave band spectra. Gordon [2] and Amick [1] have been the pioneers to formulate generic vibration criteria for vibration sensitive equipment and advanced technology facilities. These criteria were formerly known as the Bolt, Beranek and Newman (BBN) criteria and are now generally denoted as the Vibration Criteria (VC). They have been frequently used for the design of vibration sensitive facilities throughout the world.

The generic VC criteria for sensitive equipment are specified in terms of the maximum allowable RMS velocity in the one-third octave bands between 4 and 80 Hz [2]. The VC criteria impose less stringent vibration limits in the frequency range between 4 to 8 Hz, where the limit is that of constant acceleration instead of constant velocity. The VC-E criterion is the most stringent criterion, difficult to achieve in most cicumstances, and assumed to be adequate for the most demanding of sensitive systems.

3 SITE CHARACTERIZATION

The construction site is located at about 40 m from a local road (Figure 1). The (limited amount of) traffic on the nearby road determines the peak vibration levels, while the background vibration level at lower frequencies is due to the traffic on two principal roads at a further distance [3], [4].

The soil at the construction site consists of a top layer of disturbed soil with a thickness of 0.60 m, and brown peat with layers of clay and loam up to a depth of about 8 m [5]. A number of tests to determine the dynamic soil characteristics have been

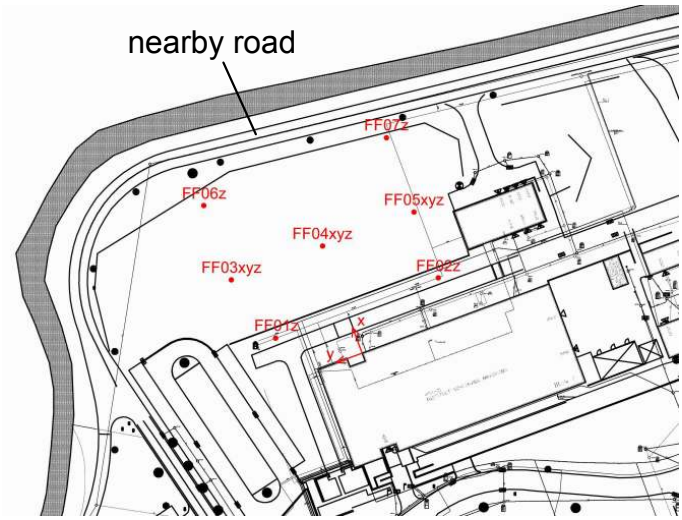

Figure 1. Location of the construction site on the Arenberg III campus of K.U.Leuven. The locations of the sensors used during monitoring of ambient vibrations are also indicated.

performed. These tests include a Seismic Cone Penetration Tests (SCPT) [6] and a Seismic Analysis of Surface Waves (SASW) [3], [4].

3.1 Dynamic soil characteristics

The SCPT has allowed for the determination of the shear wave velocity and the dilatational wave velocity of the soil from a depth of 2.3 m to a depth of 12.4 m. The dilatational wave velocity has been determined from a seismic refraction test, up to a depth of 20 m. The SASW test has allowed for the determination of the shear wave velocity of the soil up to a depth of 50 m and the material damping ratio up to a depth of 20 m.

The correspondence between the results from the SCPT, the seismic refraction test, and the SASW test is acceptable; the results can therefore be regarded as reliable. Up to a depth of about 8 m, the shear wave velocity in a number of layers is smaller than 100 m/s, which implies that the soil is very soft. This is attributed to the large amount of brown peat in the top soil layers. The soil conditions at this site are therefore not ideal for the construction of a nanotechnology facility.

Table 1. Soil profile at the site on the Arenberg III campus.

Layer	Thickness [m]	Depth [m]	C_s [m/s]	C_p [m/s]	$\beta_s = \beta_p$ [−]
1	1.18	0	128	32	0.040
2	1.12	1.18	223	42	0.040
3	1.02	2.30	88	49	0.040
4	1.53	3.32	172	41	0.040
5	3.27	4.85	97	35	0.067
6	4.74	8.12	206	140	0.007
7	5.91	12.86	247	140	0.007
8	1.23	18.77	212	157	0.007
9	5.52	20.00	212	157	0.007
10	7.23	25.52	196	157	0.007
11	∞	32.75	729	157	0.007

The resulting shear wave velocity C_s, dilatational wave velocity C_p, and material damping ratio β are shown in table 1. Furthermore, a soil density $\rho = 1750\,\mathrm{kg/m^3}$ has been assumed.

3.2 Vibration levels at the site

A vibration monitoring campaign has been performed to determine the vibration levels at the site [3], [4]. The vibration measurements have been performed during a period of more than 24 hours, using 13 seismic accelerometers installed at the soil's surface.

The analysis has been performed by computing the running RMS velocity in one-third octave bands over a period of 24 hours, with an averaging time of 4 s. This enables to efficiently represent the temporal and frequency variation of the measured vibrations. Subsequently, the statistical distribution of the RMS spectra is determined. The RMS spectra are compared with the generic vibration criteria (VC) for sensitive equipment and the ISO limit curves for human body exposure to vibrations.

Figure 2 shows the one-third octave band RMS spectra of the velocity in channel `FF06z` over a quiet period of 4 seconds on 8 January 2009 at 2h59 and over a period of 4 seconds at 8h29, during rush hour. The VC curves are superimposed on the RMS spectra. This figure confirms that the vibration levels are very low during the night time, almost one order of magnitude lower than the levels allowed by the most stringent VC-E criterion.

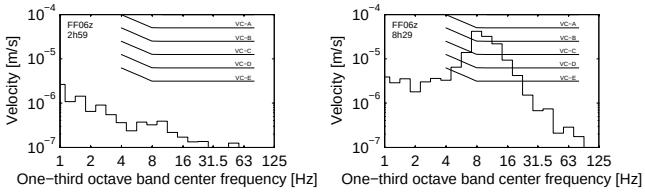

(a) (b)

Figure 2. Measured one-third octave band RMS spectra of the velocity in channels `FF06z` over a period of 4 seconds on 8 January 2009 (a) at 2h59 and (b) at 8h29.

During rush hour, the highest response is observed in the one-third octave bands with center frequencies of 8 Hz and 10 Hz, which are typical resonance frequencies of vehicle axles. In channel `FF06z`, which is probably located close to the vehicle, the vibration levels are slightly below the VC-A criterion. In the other channels, the vibration levels remain limited to the VC-C criterion or even the VC-D criterion [3].

In general, it is observed that the vibration levels are very low during the nighttime (below the VC-E criterion) but higher during daytime, especially during the morning rush hour. The peak vibration levels are due to traffic in the nearby road, leading to an exceedance of the VC-B vibration criterion in a channel located close to the road. In this channel, vibration criterion VC-B is exceeded with a probability 0.00056 (i.e. 48 seconds per day), vibration criterion VC-C with a probability 0.0019 (i.e. 3 minutes per day), vibration criterion VC-D with a probability 0.0068 (i.e. 10 minutes per day), and vibration criterion VC-E with a probability 0.052 (i.e. 76 minutes per day) [3].

4 INCIDENT WAVE FIELD

In this section, the free field response in the absence of the foundation (the incident wave field) is studied. The scenario of the passage of a truck on the nearby road is considered. It is assumed that the axle loads of the truck are applied on the surface of the halfspace, at a fixed position $\{x = 30\,\mathrm{m}, y = 0, z = 0\}^{\mathrm{T}}$. The center of the foundation is located at the origin of the Cartesian frame of reference.

The calculation of the incident wave field due to the passage of the truck consists of three steps. First, the response of the halfspace due to a unit harmonic vertical point load is computed. This is commonly denoted as a Green's function [7]. Second, the axle loads during passage of a truck on an uneven road are derived from a two-dimensional vehicle model [8]. Third, multiplication in the frequency domain of the axle loads and the Green's functions results in the response of the halfspace due to the passage of the truck.

4.1 Green's displacements

The Green's displacements of the layered halfspace are computed with the ElastoDynamics Toolbox for Matlab (EDT) [7]. Figures 3a and 4a show the incident wave field at 10 Hz and 20 Hz, respectively. The response is dominated by surface waves in the soft top layers, characterized by cylindrical wave fronts emitted from the source.

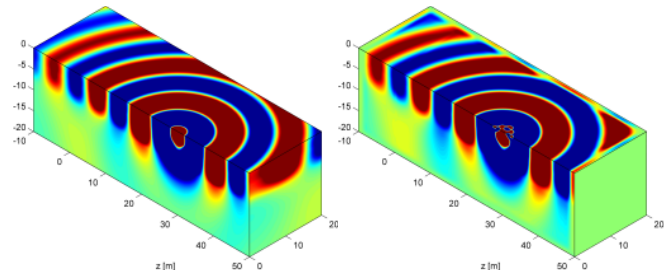

(a) (b)

Figure 3. Real part of the vertical displacement in the layered halfspace due to a unit harmonic vertical point load at $\{x = 30\,\mathrm{m}, y = 0, z = 0\}^{\mathrm{T}}$ at 10 Hz. Results computed with (a) EDT and (b) the FE-PML method are compared.

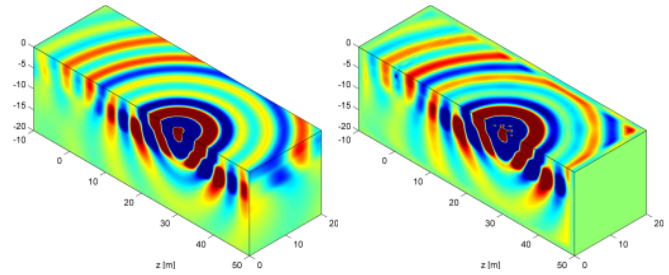

(a) (b)

Figure 4. Real part of the vertical displacement in the layered halfspace due to a unit harmonic vertical point load at $\{x = 30\,\mathrm{m}, y = 0, z = 0\}^{\mathrm{T}}$ at 20 Hz. Results computed with (a) EDT and (b) the FE-PML method are compared.

In the following section, the results of coupled FE-BE calculations will be verified by means of a second calculation, using a Perfectly Matched Layer (PML) approach. A PML is an absorbing layer that (almost) perfectly absorbs propagating waves with any angle of incidence [9], [10], [11].

The validity of the PML approach is demonstated here by comparing the Green's displacements as computed with EDT. The soil is modelled with finite elements. The soil domain is truncated at $x = -10\,\mathrm{m}$ and $x = 50\,\mathrm{m}$, $y = 0$ and $y = 20\,\mathrm{m}$, and $z = -20\,\mathrm{m}$. The truncated domain of $60\,\mathrm{m} \times 20\,\mathrm{m} \times 20\,\mathrm{m}$ is meshed with 8- node finite elements with an element side $l_{\mathrm{el}} = 1\,\mathrm{m}$. A PML with a thickness of $2\,\mathrm{m}$ is placed on the boundary of the mesh.

Figures 3 and 4 compare the Green's displacements with the results computed with EDT at 10 Hz and 20 Hz, respectively. This demonstrates the validity of the PML approach, showing no spurious reflections at the boundary of the domain. At 20 Hz, however, the wavelength in the PML solution is larger than in the reference solution. This is due to the limited size of the finite elements in the PML approach.

4.2 Dynamic axle loads

For the calculations of free field vibrations during the passage of a truck, it is assumed that the road surface on the nearby road is in very good condition and that the road unevenness is very low, corresponding to ISO 8608 class A [12].

The one-sided PSD of the unevenness is specified in terms of the wavenumber k_y as [12]:

$$G_u(k_y) = G_0 \left(\frac{k_y}{k_{y0}} \right)^{-w} \tag{1}$$

where $k_{y0} = 1\,\mathrm{rad/m}$ is the reference wavenumber, G_0 is a constant depending on the road class and w is an exponent. For a road of class A, $G_0 = 10^{-6}\,\mathrm{m^3/rad}$ and $w = 2$ [12].

From the PSD of the road unevenness, an unevenness profile is generated by considering a uniformly distributed random phase angle [8].

The passage of a two-axle VOLVO FE7 truck at a speed $v = 15\,\mathrm{m/s}$ (54 km/h) on the generated unevenness is considered. The axle loads are derived from a two-dimensional vehicle model with 4 degrees of freedom [8]. Figures 5 and 6 show the frequency content and the time history of the axle loads during a period of 4 s. The peaks in the frequency content correspond to the pitch-and-bounce modes of the vehicle at 1.3 and 1.9 Hz and the axle hop modes of the front and rear axle at 9.1 Hz and 9.3 Hz, respectively [8].

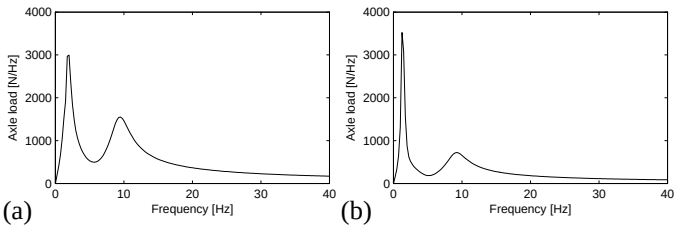

(a) (b)

Figure 5. Modulus of the Fourier transform of the axle load of (a) the front and (b) the rear axle during a period of 4 s.

The axle loads are subsequently applied at the fixed point $\{x = 30\,\mathrm{m}, y = 0, z = 0\}^{\mathrm{T}}$ at the surface of the halfspace.

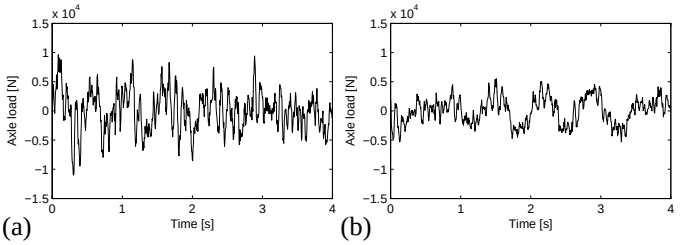

Figure 6. Time history of the axle load of the (a) front and (b) rear axle during a period of 4 s.

Figure 7 shows that the axle loads, resulting from the randomly generated unevenness (applied with a speed v to the axles), continuously generate free field vibrations from the fixed source point. The free field vibrations are therefore stationary.

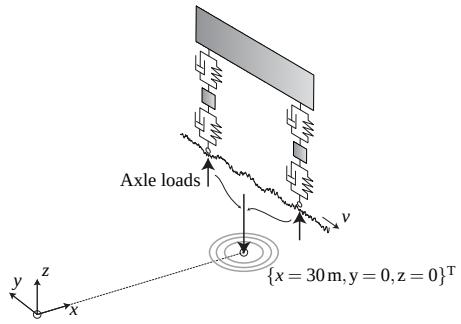

Figure 7. Application of the axle loads on the layered halfspace.

In order to demonstrate this, the frequency content and time history of the free field velocity at the surface of the layered halfspace in the origin of the Cartesian frame of reference are plotted in figures 8 and 9.

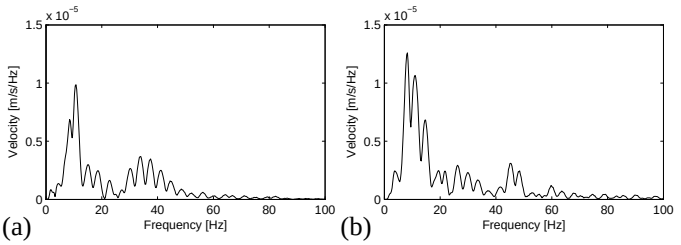

Figure 8. Modulus of (a) the horizontal and (b) the vertical velocity in the origin of the Cartesian frame of reference during the passage of the truck.

4.3 Evaluation of vibration levels

Figure 10 compares the RMS velocity spectra with the generic vibration criteria (VC) during the passage of the truck. The vertical velocity (figure 10b) should be compared with the one-third octave band RMS velocity in channel `F06z` (Figure 2), during the passage of a truck on the nearby road, since the source-receiver distances correspond. The predicted vibration levels are below the VC-C threshold, which is lower than the measured VC-B level in figure 2. This is mainly attributed to the fact that the current road unevenness is larger than the ISO 8608 class A used in the predictions.

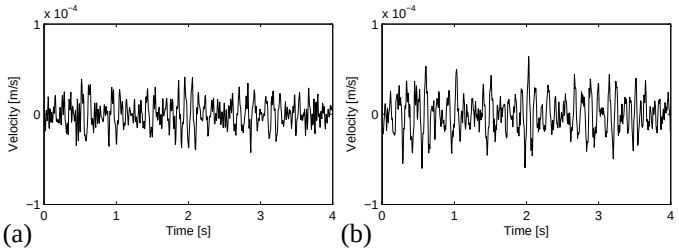

Figure 9. Time history of (a) the horizontal and (b) the vertical velocity in the origin of the Cartesian frame of reference during the passage of the truck.

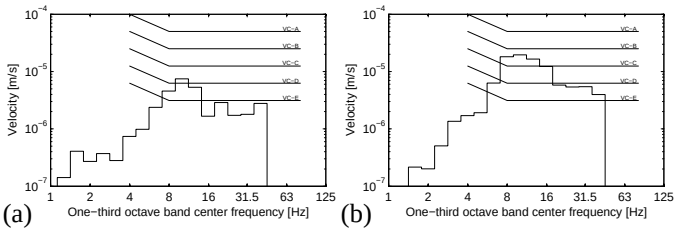

Figure 10. One-third octave band RMS (a) horizontal and (b) vertical velocity in the origin of the Cartesian frame of reference during the passage of the truck.

5 INITIAL FOUNDATION DESIGN

In the following sections, the response of different foundation designs due to the incident wave field is computed.

The initial foundation design consists of a stiff square beam grid with a side $l_b = 7.2\,\mathrm{m}$ (figure 11). The beam grid consists of concrete beams with a width $w_b = 1\,\mathrm{m}$ and a height $h_b = 1\,\mathrm{m}$. The beams are evenly spaced with a center-to-center distance of $1.8\,\mathrm{m}$, resulting in a grid of 5×5 beams. A concrete slab with a thickness $t_{sl} = 0.20\,\mathrm{m}$ is placed on the top of the beam grid. The beam grid is founded on concrete piles with a radius $R_p = 0.25\,\mathrm{m}$ up to a depth of $14\,\mathrm{m}$. The concrete of both the beam grid and the piles has a Young's modulus $E_c = 30\,\mathrm{GPa}$, a Poisson ratio $\nu_c = 0.2$, and a density $\rho_c = 2400\,\mathrm{kg/m^3}$.

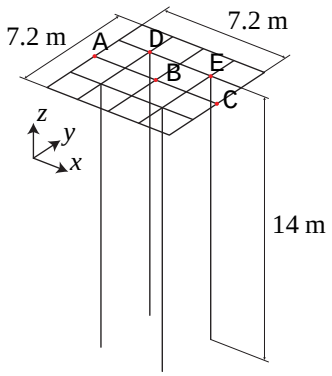

Figure 11. Foundation layout.

The response of the foundation due to a vertical harmonic point load at the surface of the layered halfspace at the point $\{x = 30\,\mathrm{m}, y = 0, z = 0\}^T$ is considered. A subdomain formulation [13] is used in order to compute the response of the foundation using a coupled FE-BE formulation, where the

dynamic interaction between the soil and the structure is fully accounted for.

5.1 Subdomain formulation

The subdomain formulation allows to write the following system of equations for the dynamic equilibrium of the foundation [13]:

$$\left(\mathbf{K}_{\mathrm{bb}} - \omega^2 \mathbf{M}_{\mathrm{bb}} + \hat{\mathbf{K}}^{\mathrm{s}}_{\mathrm{bb}}\right) \hat{\mathbf{u}}_{\mathrm{b}} = \hat{\mathbf{f}}_{\mathrm{b}} + \hat{\mathbf{f}}^{\mathrm{s}}_{\mathrm{b}} \tag{2}$$

The matrices $\mathbf{K}_{\mathrm{bb}}$ and $\mathbf{M}_{\mathrm{bb}}$ and the vector $\hat{\mathbf{f}}_{\mathrm{b}}$ correspond to the classical finite element stiffness matrix, mass matrix and force vector, respectively. The dynamic soil stiffness matrix $\hat{\mathbf{K}}^{\mathrm{s}}_{\mathrm{bb}}$ is calculated by means of a boundary element formulation. The force vector $\hat{\mathbf{f}}^{\mathrm{s}}_{\mathrm{b}}$ represents the excitation by the incident wave field on the structure and is also computed with the boundary element method [13].

In order to limit the computational effort, a modal decomposition of Q modes of the structure is used. The eigenmodes are the solution of the following generalized eigenvalue problem:

$$\mathbf{K}_{\mathrm{bb}} \boldsymbol{\psi}_{\mathbf{m}} = \omega^2_{\mathbf{m}} \mathbf{M}_{\mathrm{bb}} \boldsymbol{\psi}_{\mathbf{m}} \tag{3}$$

where ω_m, $m = 1 \ldots Q$ are the corresponding eigenfrequencies.

The structural displacement vector $\hat{\mathbf{u}}_{\mathrm{b}}$ is decomposed onto the modal basis as:

$$\hat{\mathbf{u}}_{\mathrm{b}} = \sum_{m=1}^{Q} \hat{\alpha}_m \boldsymbol{\psi}_m \tag{4}$$

The modes $\boldsymbol{\psi}_m$, $m = 1 \ldots Q$ are collected in a matrix $\boldsymbol{\Psi}$:

$$\hat{\mathbf{u}}_{\mathrm{b}} = \boldsymbol{\Psi} \hat{\alpha} \tag{5}$$

where the vector $\hat{\alpha}$ collects the modal coordinates $\hat{\alpha}_m$. Introducing the modal decomposition (5) into the equation of motion (2) results in [14]:

$$\left(\boldsymbol{\Lambda}_{QQ} - \omega^2 \mathbf{I}_{\mathbf{QQ}} + \boldsymbol{\Psi}^{\mathrm{T}} \hat{\mathbf{K}}^{\mathrm{s}}_{\mathrm{bb}} \boldsymbol{\Psi}\right) \hat{\alpha} = \boldsymbol{\Psi}^{\mathrm{T}} \left(\hat{\mathbf{f}}_{\mathrm{b}} + \hat{\mathbf{f}}^{\mathrm{s}}_{\mathrm{b}}\right) \tag{6}$$

where the Q-dimensional matrix $\boldsymbol{\Lambda}_{QQ}$ contains the squares of the eigenfrequencies ω_m, $m = 1 \ldots Q$. The Q-dimensional unit matrix $\mathbf{I}_{\mathbf{QQ}}$ reflects the orthogonality of the eigenmodes with respect to the mass matrix.

In the present calculation, $Q = 100$ eigenmodes are considered. The eigenfrequency of mode 100 equals 194.32 Hz, so that the number of modes is sufficient for calculation in the frequency range 1-40 Hz under consideration [15]. The modes are characterized by flexural modes of the piles (figure 12). A significant deformation of the stiff beam grid is only observed above a frequency of 50 Hz. It is therefore expected that the beam grid behaves as a rigid body at lower frequencies.

5.2 Response

The subdomain formulation is employed to compute the response due to a unit harmonic vertical point load at the surface of the layered halfspace at the point $\{x = 30\,\mathrm{m}, \mathrm{y} = 0, \mathrm{z} = 0\}^{\mathrm{T}}$. In the case where the dynamic interaction between the foundation and the soil is accounted for, the soil displacements differ from the incident wave field, especially in the vicinity of the foundation. The vertical displacements in figure 13 show a reduction of vibration levels behind the foundation (at $x < 0$), which demonstrates the screening effect of the foundation.

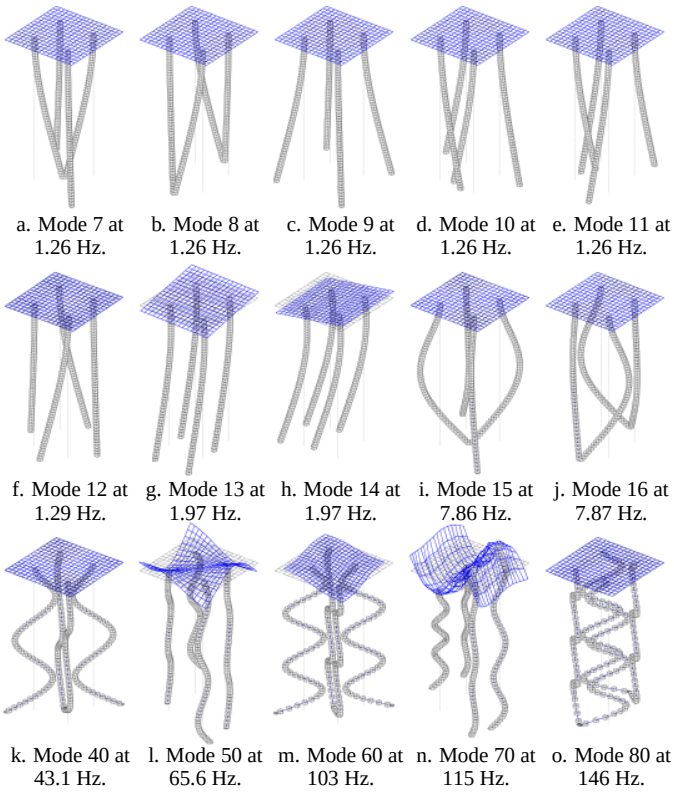

a. Mode 7 at 1.26 Hz. b. Mode 8 at 1.26 Hz. c. Mode 9 at 1.26 Hz. d. Mode 10 at 1.26 Hz. e. Mode 11 at 1.26 Hz.

f. Mode 12 at 1.29 Hz. g. Mode 13 at 1.97 Hz. h. Mode 14 at 1.97 Hz. i. Mode 15 at 7.86 Hz. j. Mode 16 at 7.87 Hz.

k. Mode 40 at 43.1 Hz. l. Mode 50 at 65.6 Hz. m. Mode 60 at 103 Hz. n. Mode 70 at 115 Hz. o. Mode 80 at 146 Hz.

Figure 12. Structural modes for case 1.

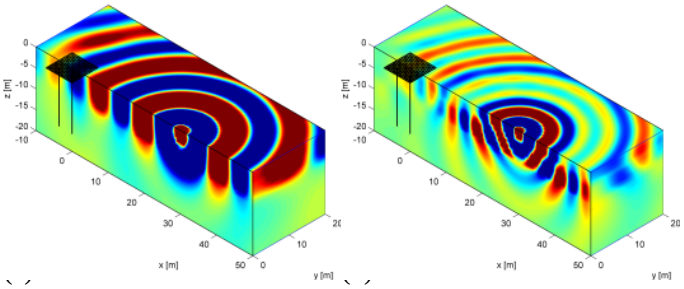

Figure 13. Real part of the vertical displacement in the layered halfspace (in presence of the foundation) due to a unit harmonic vertical point load at $\{x = 30\,\mathrm{m}, \mathrm{y} = 0, \mathrm{z} = 0\}^{\mathrm{T}}$ at (a) 10 Hz and (b) 20 Hz. The dynamic interaction between the soil and the foundation is fully accounted for.

Figures 16 and 17 show the real and imaginary part of the foundation displacement at 10 Hz. This demonstrates that the incident wave field is imposed to the pile, resulting in bending of the piles. The beam grid deforms as a rigid body, where a predominant rigid body rotation is observed.

5.3 Transfer function

The transfer function between the unit harmonic vertical point load at the surface of the layered halfspace at the point $\{x = 30\,\mathrm{m}, \mathrm{y} = 0, \mathrm{z} = 0\}^{\mathrm{T}}$ and the structural velocity, referred to as the mobility, is next computed in the frequency range from 0 to 40 Hz. Figures 18 and 19 show the modulus of the horizontal

and vertical velocity in the points A to E (figure 11). As a result of the rigid body rotation of the beam grid, the vertical displacement in the points A, C, D, and E is significantly larger than in the point B in the center of the beam grid.

5.4 *Verification*

Next, the response of the foundation is computed using the PML approach. Figures 14 and 15 show the vertical displacement in the soil, which are in correspondance with the results obtained in the previous section using the coupled FE-BE method (figure 13).

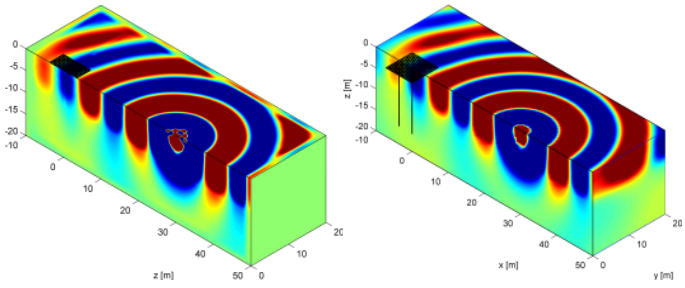

(a) (b)

Figure 14. Real part of the vertical displacements in the soil at 10 Hz. The results (a) computed with the PML approach are compared to (b) the coupled FE-BE results.

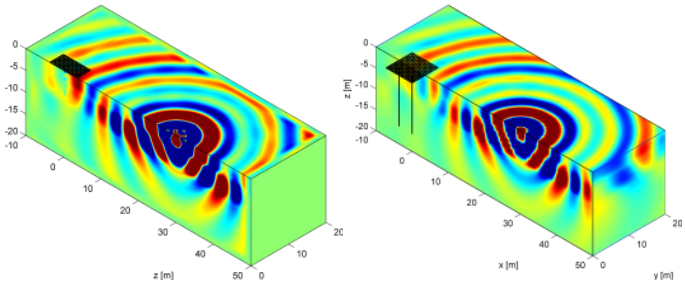

(a) (b)

Figure 15. Real part of the vertical displacements in the soil at 20 Hz. The results (a) computed with the PML approach are compared to (b) the coupled FE-BE results.

5.5 *Evaluation of vibration levels*

The transfer function between the vertical point load at the surface of the layered halfspace and the response of the foundation is used to assess the vibration performance of the foundation.

Figures 20 and 21 show the one-third octave band RMS spectra of the horizontal and vertical velocity during the passage of the truck. A comparison with the VC vibration criteria shows that only VC-B is met. This is mainly due to the fact that the large vibration levels in the soft top soil layers are imposed on the piles. In order to achieve a better vibration performance, a larger pile diameter of 0.4 m (case 2) and 0.5 m (case 3) is considered, in an attempt to reduce the vibration levels.

6 MODIFIED FOUNDATION DESIGN

Figures 16 and 17 show the deformation for the different foundation designs at 10 Hz. The increased bending stiffness of the piles of cases 2 and 3 with respect to case 1 results in smaller deformations of the piles. This is also observed in figures 18 and 19 that compare the mobility for cases 1 to 3. Mainly the rigid body rotation of the beam grid, that results in large vertical displacements in the points A, C, D, and E, is strongly reduced.

A significant reduction of the vibration levels is achieved for a pile with a radius of 0.40 m. Case 2 satisfies the VC-C criterion. Further increasing the pile up to a radius $r_\mathrm{p} = 0.50\,\mathrm{m}$ results in a small additional reduction of the vibration levels. Case 3 satisfies the VC-C criterion.

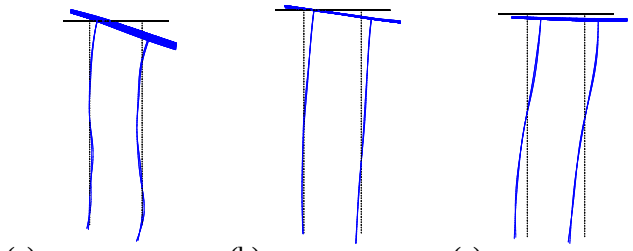

(a) (b) (c)

Figure 16. Real part of the displacement of the foundation for (a) case 1, (b) case 2 and (c) case 3 due to a unit harmonic vertical point load at $\{x = 30\,\mathrm{m}, \mathrm{y} = 0, \mathrm{z} = 0\}^\mathrm{T}$ at 10 Hz (displacement scale 1×10^{10}).

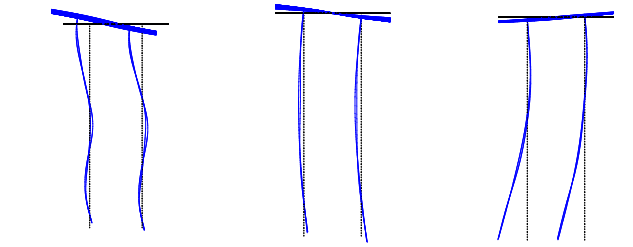

(a) (b) (c)

Figure 17. Imaginary part of the displacement of the foundation for (a) case 1, (b) case 2 and (c) case 3 due to a unit harmonic vertical point load at $\{x = 30\,\mathrm{m}, \mathrm{y} = 0, \mathrm{z} = 0\}^\mathrm{T}$ at 10 Hz (displacement scale 1×10^{10}).

However, this exceedance will only occur during the passage of a truck on the nearby road. The results should be interpreted statistically (as has also been done for the in situ measurements), taking into account the expected amount of traffic on the nearby road. Low vibration levels that meet the VC-E criterion are expected during the largest part of day and night [3], [4], while larger vibration levels occur during rush hours.

In this sence, the computed transfer functions allow to compare the incident wave field and the foundation response for different foundation designs. The transfer function for cases 2 and 3 is smaller than the incident wave field, especially in the vertical direction. This indicates that the low vibration levels (below VC-E) during quiet periods of day or night are expected to be preserved after construction of the foundation.

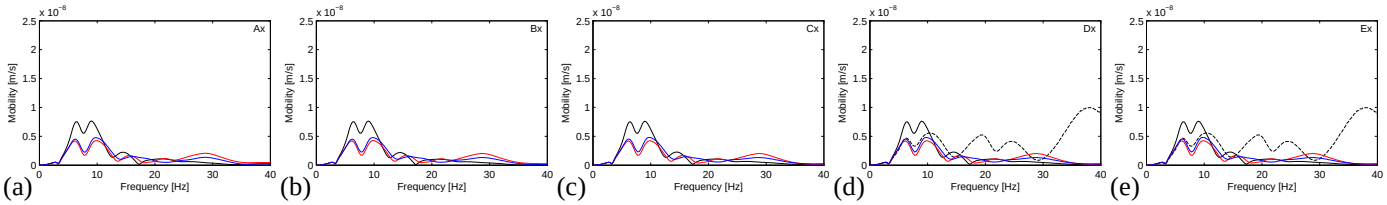

Figure 18. Modulus of the horizontal velocity in the points (a) A, (b) B, (c) C, (d) D, and (e) E. The results for case 1 (black line), case 2 (blue line) and case 3 (red line) are compared. The incident wave field on the pile heads is plotted with dashed lines.

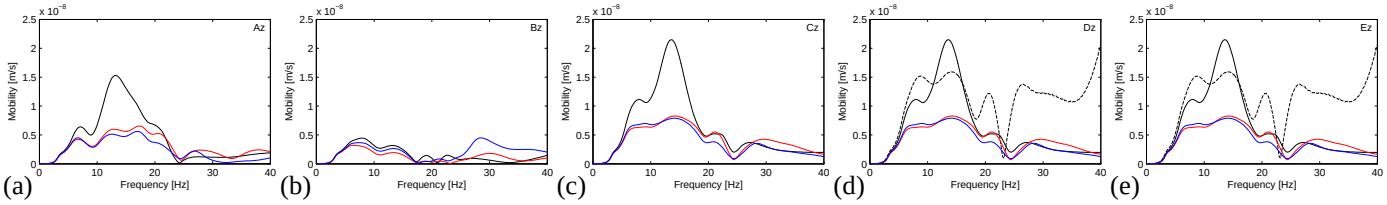

Figure 19. Modulus of the vertical velocity during the passage of the truck in the points (a) A, (b) B, (c) C, (d) D, and (e) E. The results for case 1 (black line), case 2 (blue line) and case 3 (red line) are compared. The incident wave field on the pile heads is plotted with dashed lines.

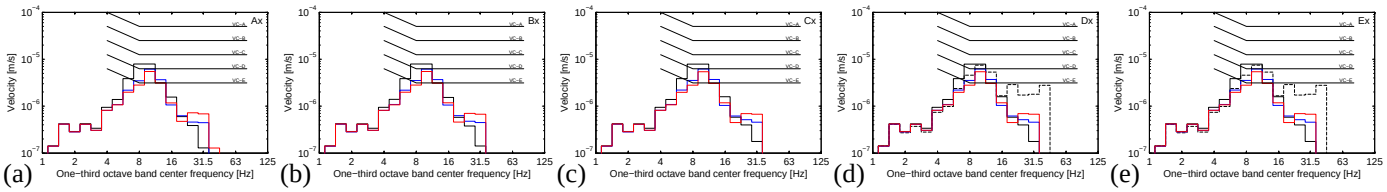

Figure 20. One-third octave band RMS horizontal velocity during the passage of the truck in the points (a) A, (b) B, (c) C, (d) D, and (e) E. The results for case 1 (black line), case 2 (blue line) and case 3 (red line) are compared. The incident wave field on the pile heads is plotted with dashed lines.

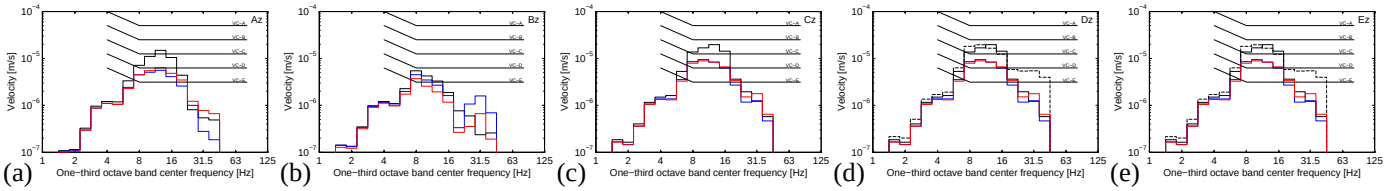

Figure 21. One-third octave band RMS vertical velocity in the points (a) A, (b) B, (c) C, (d) D, and (e) E. The results for case 1 (black line), case 2 (blue line) and case 3 (red line) are compared. The incident wave field on the pile heads is plotted with dashed lines.

7 CONCLUSION

In this paper, the dynamic response of the piled foundation of the Corelab 1B nanotechnology facility has been investigated.

First, the transfer function between a vertical force on a nearby road and the foundation has been computed using a coupled finite element - boundary element method, where the dynamic soil-structure interaction is fully accounted for. The structure is modelled with finite elements while the soil is modelled with boundary elements. The results are verified by means of a FE calculation where the wave field in the soil is absorbed using a Perfectly Matched Layer technique.

In case 1, the piles with a radius $r_p = 0.25\,\mathrm{m}$ are strongly deformed by the incident wave field in the soft top soil layer of 8 m, due to the relatively low bending stiffness of the piles. This results in large rigid body rotation of the beam grid, with corresponding large vertical displacements. In cases 2 and 3, a significant reduction of the vibration levels is achieved, due to the increased bending stiffness of the piles.

The computed transfer functions allow to compare the incident wave field and the foundation response for different foundation designs. The transfer function for cases 2 and 3 is smaller than the incident wave field, especially in the vertical direction. This indicates that the low vibration levels (below VC-E) during quiet periods of day or night are expected to be preserved after construction of the foundation. These low vibration levels occur during the largest part of the day, as vibration monitoring has shown that the VC-E criterion is only exceeded during 76 minutes per day.

REFERENCES

[1] H. Amick, "On generic vibration criteria for advanced technology facilities," *Journal of the Institute of Environmental Sciences*, vol. 40, pp. 35–44, 1997.

[2] C.G. Gordon, "Generic criteria for vibration-sensitive equipment," in *Proceedings of the SPIE Conference on Vibration Control and Metrology*, San Jose, California, USA, November 1991, vol. 1619, pp. 71–85.
[3] M. Schevenels and G. Degrande, "Site vibration evaluation on the Arenberg campus for the planning of a nanotechnology laboratory: a comparison of three sites," Tech. Rep. BWM-2009-10, Department of Civil Engineering, K.U.Leuven, April 2009.
[4] M. Schevenels and G. Degrande, "Site vibration evaluation on the Arenberg III campus for the planning of a nanotechnology laboratory," Tech. Rep. BWM-2009-04, Department of Civil Engineering, K.U.Leuven, March 2009.
[5] "Databank Ondergrond Vlaanderen," http://dov.vlaanderen.be.
[6] L. Areias, "Seismic cone test SCPT1, Arenberg III campus, Celestijnenlaan, Heverlee," Technical report, iGeotechnics, February 2009.
[7] M. Schevenels, S. François, and G. Degrande, "EDT: An ElastoDynamics Toolbox for MATLAB," *Computers & Geosciences*, vol. 35, no. 8, pp. 1752–1754, 2009.
[8] G. Lombaert, *Development and experimental validation of a numerical model for the free field vibrations induced by road traffic*, Ph.D. thesis, Department of Civil Engineering, K.U.Leuven, 2001.
[9] J.P. Bérenger, "A perfectly matched layer for the absorption of electromagnetic waves," *Journal of Computational Physics*, vol. 41, pp. 115–135, 1994.
[10] W.C. Chew and Q.H. Liu, "Perfectly matched layers for elastodynamics: A new absorbing boundary condition," *Journal of Computational Acoustics*, vol. 4, no. 4, pp. 341–359, 1996.
[11] U. Basu and A.K. Chopra, "Perfectly matched layers for time-harmonic elastodynamics of unbounded domains: theory and finite-element implementation," *Computer Methods in Applied Mechanics and Engineering*, vol. 192, no. 11-12, pp. 1337–1375, 2003.
[12] ISO/DIS 8608, "Vibration mécaniques - profils de routes - méthode de presentation des résultats de mesures," Norme internationale, Organisation internationale de normalisation, 1991.
[13] S. François, *Nonlinear modelling of the response of structures due to ground vibrations*, Ph.D. thesis, Department of Civil Engineering, K.U.Leuven, 2008.
[14] L. Pyl, *Development and experimental validation of a numerical model for traffic induced vibrations in buildings*, Ph.D. thesis, Department of Civil Engineering, K.U.Leuven, 2004.
[15] S. Rubin, "Improved component-mode representation for structural dynamic analysis," *AIAA Journal*, vol. 13, no. 8, pp. 995–1006, August 1975.